

# Cascading failures in isotropic and anisotropic spatial networks induced by localized attacks and overloads

Ignacio A. Perez,<sup>1,\*</sup> Dana Vaknin Ben Porath,<sup>2</sup> Cristian E. La Rocca,<sup>1</sup>  
Sergey V. Buldyrev,<sup>3,4</sup> Lidia A. Braunstein,<sup>1,4</sup> and Shlomo Havlin<sup>2,4</sup>

<sup>1</sup>*Instituto de Investigaciones Físicas de Mar del Plata (IFIMAR)-Departamento de Física,  
FCEyN, Universidad Nacional de Mar del Plata-CONICET,  
Deán Funes 3350, (7600) Mar del Plata, Argentina*

<sup>2</sup>*Department of Physics, Bar-Ilan University, Ramat-Gan 52900, Israel*

<sup>3</sup>*Department of Physics, Yeshiva University, New York 10033, USA*

<sup>4</sup>*Physics Department, Boston University,  
590 Commonwealth Ave., Boston, Massachusetts 02215, USA*

## Abstract

Cascading failures are catastrophic processes that can destroy the functionality of a system, thus, understanding their development in real infrastructures is of vital importance. This may lead to a better management of everyday complex infrastructures relevant to modern societies, e.g., electrical power grids, communication and traffic networks. In this paper we examine the Motter-Lai model [1] of cascading failures induced by overloads in both isotropic and anisotropic spatial networks, generated by placing nodes in a square lattice and using various distributions of link lengths and angles. Anisotropy has not been earlier considered in the Motter-Lai model and is a real feature that may affect the cascading failures. This could reflect the existence of a preferred direction in which a given attribute of the system manifests, such as power lines that follow a city built parallel to the coast. We analyze the evolution of the cascading failures for systems with different strengths of anisotropy and show that the anisotropy causes a greater spread of damage along the preferential direction of links. We identify the *critical linear size*,  $l_c$ , for a square shaped localized attack, which satisfies with high probability that above  $l_c$  the cascading disrupts the giant component of functional nodes, while below  $l_c$  the damage does not spread. We find that, for networks with any characteristic link length, their robustness decreases with the strength of the anisotropy. We show that the value of  $l_c$  is finite and independent of the system size (for large systems), both for isotropic and anisotropic networks. Thus, in contrast to random attacks, where the critical fraction of nodes that survive the initial attack,  $p_c$ , is usually below 1, here  $p_c = 1$ . Note that the analogy to  $p_c = 1$  is also found for localized attacks in interdependent spatial networks [2]. Finally, we measure the final distribution of functional cluster sizes and find a power-law behavior, with exponents similar to regular percolation. This indicates that, after the cascade which destroys the giant component, the system is at a percolation critical point. Additionally, we observe a crossover in the value of the distribution exponent, from critical percolation in a two-dimensional lattice for strong spatial embedding, to mean-field percolation for weak embedding.

---

\* ignacioperez@mdp.edu.ar

## I. INTRODUCTION

Real-world infrastructures such as power grids, sewer networks, and telecommunication systems can be particularly affected by a process known as cascading failures (CF). This is a dynamic process in which the malfunction of one or a few components of the system leads to the failure of other components, and so on, and could cause a large fraction of the system to collapse. Motter and Lai [1] modeled the process of CF induced by overloads. In their model, at each time step, some relevant physical quantity (e.g., energy or information) is exchanged between every pair of nodes and transmitted along the shortest path [3, 4] between them. Then, the load  $L_i$  at node  $i$  is defined as the total number of shortest paths passing through this node, and the capacity  $C_i$  is the maximum load that the node can handle. Since in man-made networks capacity is limited by cost, Motter and Lai [1] assumed that the capacity of node  $i$  is proportional to the original load  $L_i^0$ , i.e.,  $C_i = (1 + \alpha)L_i^0$ , where the constant  $\alpha \geq 0$  is the *tolerance* of the system to overloads. The failures of nodes cause the redistribution of shortest paths. As a result, the load at some nodes can increase and exceed their capacities  $C_i$ . These overloaded nodes then fail and, since the shortest paths change, this may cause further overloads and subsequent failures, in a cascade manner [5]. This kind of CF can be catastrophic, meaning that even a small amount of initial failures can damage a substantial portion of the system, and eventually cause its total collapse [1, 6–8].

Usually, infrastructures are embedded in space, and thus several models of CF in spatially-embedded networks have been proposed for approaching this problem [9, 10]. Zhao et al. [9] modeled a cascade of failures induced by overloads in a square lattice. They triggered the cascade with a localized attack, which usually occurs in natural catastrophes or malicious attacks by removing nodes at the center of the network. They found that failures spread radially from the center of the initial attack with an approximately constant velocity, which decreases with increasing tolerance. However, real systems are rarely found to be perfect lattices and present, instead, a characteristic euclidean link length  $\zeta$ , such as the European power grid and the inter station local railway lines in Japan [11–13]. This feature can be modeled by assuming that links connecting different nodes in a lattice have a link length distribution  $P(r) \sim \exp(-r/\zeta)$  [11], where  $r$  is the Euclidean distance between two nodes and  $\zeta$  determines the typical length of links in the spatial embedding. For  $\zeta \rightarrow \infty$  all link lengths are equally likely and spatial effects vanish, while for smaller values of  $\zeta$  the

strength of the spatial embedding increases, as shorter link lengths are favored.

Within spatial networks, a prominent characteristic of many real infrastructures (e.g., grids, pipeline systems, and transportation networks) is the presence of anisotropy in the orientation of the connections between nodes. Usually, the disposition of links is not the same in all directions, they rather follow the distribution of the population, which can be anisotropic since, in many cases, it spreads along geographical landscapes (e.g., rivers, sea coasts, mountain ranges) or major transportation routes. It is expected that these deviation from an isotropic lattice will change significantly the characteristics of CF spread.

In this paper we study both the critical damage size that will disrupt a spatially-embedded network and the effects of anisotropy in the embedding on CF induced by overloads. Without loss of generality, we study here the case where the overload failures are triggered by a square shaped, localized attack at the center of the network. We introduce anisotropy as a preferential direction in which links are more likely to form. We find that, although anisotropy hinders the propagation of failures along the orthogonal direction, it deteriorates the overall robustness of the system, and that the initial critical damage size is independent of the system size. Analyzing the distribution of functional cluster sizes,  $n_s$ , at the end of the CF, we find that, as a result of the network fragmentation, the distribution behaves like a power-law,  $n_s \sim s^{-\tau}$ . Furthermore, we observe a crossover for the exponent  $\tau$ , which changes from the known exponent value of critical percolation in two-dimensional lattices, for high spatial embedding, to the mean field value as the embedding declines.

## II. THE $\zeta$ -MODEL

We model the process of CF produced by spreading of overloads, in a spatially-embedded and weighted network, which we call the  $\zeta$ -model [14]. The nodes of the network are placed in the vertices of a square lattice of size  $L \times L$ . The lengths,  $r$ , of the links are taken from the distribution  $P(r) \sim \exp(-r/\zeta)$ . That is,  $\zeta$  is the characteristic length of the links. Also, we use here rigid boundary conditions, but similar results can be obtained for periodic boundary conditions. To model the isotropy and the anisotropy, the directions of links (i.e., the angles  $\theta$  that links form with the horizontal axis), are taken from a uniform distribution  $U_{[0,2\pi)}$  or a Gaussian distribution  $N(\theta_p, \sigma^2)$ , where  $\theta$  and  $\theta + 2\pi$  correspond to the same direction. In the anisotropic distribution,  $N(\theta_p, \sigma^2)$ , the angle  $\theta_p$  represents the preferential direction for the

connections, while  $\sigma$  is the corresponding standard deviation, which controls the strength of the anisotropy. For instance,  $\sigma \rightarrow 0$  represents the case of a unique possible angle for the connections between nodes, while  $\sigma \rightarrow \infty$  corresponds to an isotropic network, where links appear with equal probability in all directions. The weight of a link represents, e.g., the time needed to traverse it, if the optimal path is defined as the path with a minimal travel time. We take the weights, which are independent of  $r$ , from a Gaussian distribution  $N_\omega(\omega^*, \sigma_\omega^2)$ , where  $\omega^*$  is the average weight and  $\sigma_\omega$  is the corresponding standard deviation.

To construct the  $\zeta$ -model network, we assign  $(x, y)$  integer coordinates ( $x, y \in [1, L]$ ) for each of the  $N = L \times L$  nodes. Then we select, at random, a node  $i$  with coordinates  $(x_i, y_i)$  and draw a ray of length  $r$  and angle  $\theta$  above the horizontal axis, which are randomly selected from the distributions  $P(r)$  and  $N(\theta_p, \sigma^2)$ , respectively. Next, we connect the node  $i$  with the node  $j$  that is closest to the end point of the ray,  $p$ , with real coordinates  $(p_x, p_y) = (x_i + r\cos\theta, y_i + r\sin\theta)$  (see Fig. 1 (a)), and assign to the link a weight  $\omega$  from the distribution  $N_\omega(\omega^*, \sigma_\omega^2)$ . We repeat the process until the total number of links in the network is  $N\langle k\rangle/2$ , where  $\langle k\rangle$  is the average number of links per node (self and multiple links are not allowed). In Figs. 1 (b) and (c), we show representations of anisotropic and isotropic networks, respectively.

The dynamic process of CF develops as follows. Initially, at time  $t = 0$ , all nodes are functional, and the load at node  $i$  is  $L_i^0 \equiv L_i(t = 0)$ , which is computed as the total number of optimal paths [1, 15] between all pairs of nodes that pass through node  $i$ . Then, the capacity of node  $i$ ,  $C_i$ , is defined as  $C_i = (1 + \alpha)L_i^0$ , where  $\alpha$  is the homogeneous (i.e., the same for all nodes) tolerance of the system to overloads. We assume that  $\alpha$ , and thus  $C_i$ , are constants throughout the entire process. At time  $t = 1$ , we generate a square shaped, localized attack of  $\Delta l = l \times l$  nodes which fail at the center of the network. Due to this attack, the optimal paths may be redistributed, changing the load of some nodes. Then, at time  $t > 1$ , all nodes fail if their loads (which must be computed at every single time step) are above their capacities, i.e., if  $L_i(t) > C_i$ . The process continues until the failures produced at a given time step cause no new nodes to fail at a posterior time.

It is important to note that initially, the giant component (GC) in the network (i. e., the biggest group of nodes where each node has a path to each other) spans the system reaching all four boundaries.

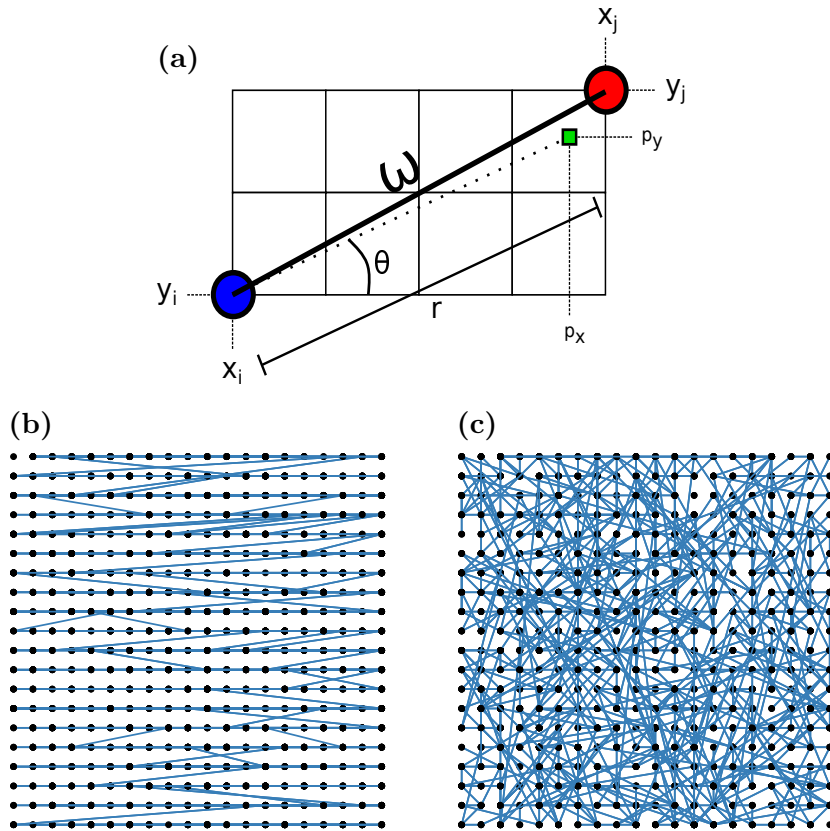


FIG. 1. (a) Constructing the network's links. First, a node  $i$  with coordinates  $(x_i, y_i)$  in the lattice (blue circle) is selected at random. A link is created between this node and node  $j$  (red circle), which is the closest node to the site  $(p_x, p_y) = (x_i + r\cos\theta, y_i + r\sin\theta)$  marked as a green square. The link is represented with a straight line and is assigned a weight  $\omega$ . Nodes in the remaining sites of the lattice are not shown for clarity. In the bottom figures, we show two different networks from our model with: (b) high anisotropy ( $\sigma = 0.05$ ) and (c) isotropy, both for  $L = 20$  and  $\zeta = 3$ .

### III. RESULTS

Before presenting the actual results of this study, we note that in the limit of an isotropic network ( $\sigma \rightarrow \infty$ ) and for small values of  $\zeta$  (e.g.,  $\zeta = 1$ ), our model coincides with the lattice model of Ref. [9]. In the Supplementary Information section, we provide results that support this statement. For all simulations (including those in the SI section) we use, without loss of generality,  $\langle k \rangle = 4$ ,  $\theta_p = 0$ ,  $\omega^* = 5$ , and  $\sigma_\omega = 0.1$ .

Now, we begin with the analysis of our model and study the evolution of the cascade and the spatial distribution of the failures for a fixed size of the initial attack, in networks

with different degrees of anisotropy. We denote the number of nodes that fail at time  $t$  as  $F_t \equiv F(t)$ , while  $R_p \equiv R_p(t)$  and  $R_o \equiv R_o(t)$  are the standard deviations of the coordinates of all nodes failed during all time steps from 0 to  $t$ , in the preferential (horizontal) and orthogonal directions, respectively.

In Figs. 2 (a) and (b), we show  $F_t$ ,  $R_p$ , and  $R_o$  for networks with  $L = 200$ ,  $\zeta = 3$ ,  $\alpha = 0.25$ ,  $l = 6$ , and different values of  $\sigma$ . We observe that the initial attack produces a CF in the network, where the maximum amount of failing nodes at a certain time  $t$  - the peak value of  $F_t$  in Fig. 2 (a) - increases with increasing  $\sigma$ , i.e., as the strength of the anisotropy decreases. In this way, fewer nodes will remain functional due to overloads, at the end of the cascading, in the isotropic case, as compared to the anisotropic case. Also, anisotropy affects the spatial distribution of failures over time, limiting the propagation in the orthogonal direction ( $\theta = \pi/2$ ) compared to that in the preferred direction ( $\theta_p = 0$ ), i.e.,  $R_o < R_p$  (see Fig. 2 (b)). However, as  $\sigma$  increases and the network loses its characteristic anisotropy, the gap between the extents along the two directions becomes smaller.

Additionally, in Figs. 2 (c) and (d), we plot the ratio  $R_o^\infty/R_p^\infty$  ( $R^\infty \equiv R(t \rightarrow \infty)$ ) and the final distribution of failures in the network, respectively, which help in clarifying the effects of anisotropy at the end of the cascade process. In Fig. 2 (c), we observe a convergence towards a final isotropic state ( $R_o^\infty/R_p^\infty \rightarrow 1$ ) for large values of  $\sigma$ . For high anisotropy (small  $\sigma$ ), the observed ratio approaches zero and the damage does not spread vertically. This is since the shortage of vertical links makes them to break at early stages due to overloads (see Fig. 8 of the SI section, where we show the same behavior for other  $\alpha$  values). Finally, in Fig. 2 (d) we depict examples of the spread of failures for different degrees of anisotropy and particular realizations of the cascade process. This gives us a visual image of the total damage caused by the initial attack, and how it is reduced in the orthogonal direction as the anisotropy increases (i.e., as  $\sigma$  decreases).

In light of these results, one might be tempted to conclude that systems with a structural anisotropy are more robust against localized attacks, compared to isotropic systems. However, measures such as the total amount of failures or their spatial extension might not be the most relevant for revealing the effects that anisotropy produces in the systems that we are exploring. In particular, note that in Fig. 2 (d), while the damage is the smallest for  $\sigma = 0.05$ , the system is no longer functional since the giant component is vertically broken.

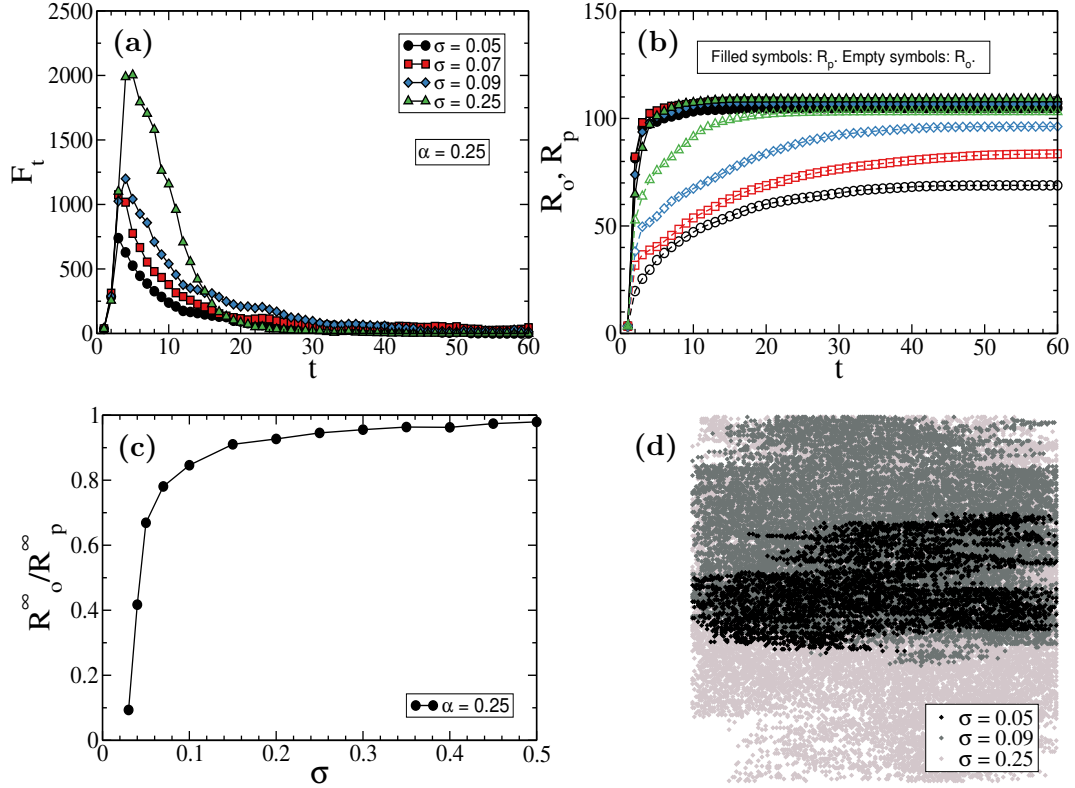


FIG. 2. (a) Number of failures,  $F_t$ , as a function of time  $t$ , for different values of  $\sigma$ . (b) Evaluating the extent of the failures in the preferential and orthogonal directions,  $R_p$  and  $R_o$ , respectively, for the same values of the parameters shown in (a). (c) Ratio  $R_o^\infty / R_p^\infty$  between the extent of the failures in each direction, at the end of the cascade. (d) Demonstrating individual realizations of the network showing the final spatial distribution of failed nodes (the exact disposition of failures may vary slightly between realizations). Anisotropy favors the propagation of failures along the preferred horizontal direction ( $\theta_p = 0$ ) over the orthogonal direction. This is since the rare vertical links become overloaded and fail at the beginning of the cascade. The parameters of the simulations are  $L = 200$ ,  $\zeta = 3$ ,  $\alpha = 0.25$ , and  $l = 6$ . Results in (a), (b), and (c), have been averaged over  $N_{rea} = 35$  realizations. Note that all networks have initially (before the localized attack) a GC that spans the entire system, all four edges.

Next we ask what is the critical linear size of attack  $l_c$ , for a given tolerance  $\alpha$ , such that above this value the GC of functional nodes, at the end of the cascade, breaks down (red region in Fig. 3 (a)), and below it the damage is only localized (green region in Fig. 3 (a)). We define the critical condition for computing  $l_c$  as follows. For isotropic systems,  $l_c$  defines



the limit where the GC, above this value, does not reach, at least, one of the four edges of the network. For anisotropic systems, attacks with  $l > l_c$  will break the GC in the vertical direction, i.e., the GC will not reach, at least, the upper edge or the bottom edge of the network. We make this distinction because, in anisotropic networks, links are more abundant along the preferred direction ( $\theta_p = 0$  in this case) than along the perpendicular direction. Therefore, it is more likely for the GC to break apart due to failures that propagate vertically throughout the system. It is worth mentioning that, in order to get the values of  $l_c(\alpha)$ , we generate 20 realizations of networks and, for each attack size  $l$ , we use a binary search to detect the critical tolerance,  $\alpha_c$ . Then, we average the results of  $\alpha_c$  for the different networks (we show dispersion values in Fig. 11, in the SI section), obtaining the curve  $\alpha_c(l)$ , which we adjust to present as  $l_c(\alpha)$ . Accordingly, the probability of complete destruction of the GC sharply increases near  $l_c$ .

First we present, in Fig. 3 (b), the critical linear size of attack  $l_c(\alpha)$  for the isotropic case and different values of the system size  $L$  and the characteristic link length  $\zeta$ . For attack sizes that are below these curves, i.e.,  $l < l_c(\alpha)$  (recall Fig. 3 (a)), the GC spans the entire system, both along the preferred (horizontal) and the orthogonal direction, while above  $l_c(\alpha)$  it does not, i.e., the GC breaks and can not reach, at least, one edge of the network. We can see that the critical size  $l_c$  increases with the tolerance  $\alpha$ , since nodes with larger capacities are less likely to become overloaded and fail, thus making the network more robust against the attacks. It is interesting to note that the critical size  $l_c$  does not depend on the system linear size,  $L$ , in the limit  $L \rightarrow \infty$ . Thus a zero fraction (microscopic) of localized failures yields a macroscopic transition. This is analogous to a similar behavior found in percolation of interdependent spatial networks [2, 16], and is in marked contrast with random failures for which the removal of a finite fraction of the system is needed to cause full collapse. We also observe that the spatial embedding triggers and enhance the propagation of the failures in the system. Note that the critical initial damage size decreases with decreasing the typical link length  $\zeta$ , thus smaller attack sizes can trigger the more spatial systems to collapse (see Fig. 3).

Next, we analyze anisotropic systems, for which results are shown in Figs. 3 (c) and (d), and correspond to  $\zeta = 3$  and  $\zeta = 10$ , respectively. We show results for two different values of the anisotropy parameter,  $\sigma = 0.25, 1$ , in order to depict networks with rather different degrees of anisotropy. Note that, in this case, attack sizes above the critical value  $l_c$  produce

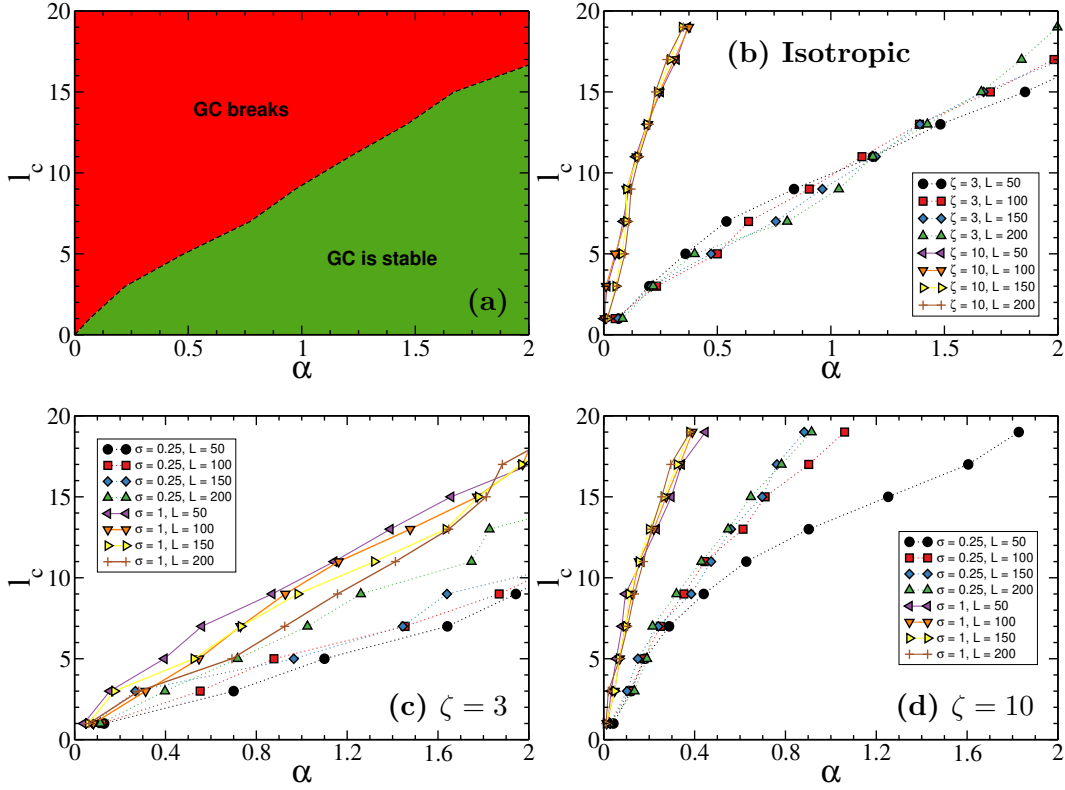


FIG. 3. Robustness of the system against localized attacks. (a) Scheme of a critical curve for the linear attack size  $l_c$  as function of the tolerance  $\alpha$ . Below the curve (green region), the GC holds stable and the damage is only localized. Above the curve (red region), the functional GC breaks down, i.e., it can not reach, at least, one of the network edges (isotropic networks) or it can not extend throughout all the vertical length of the system (anisotropic networks). (b) Critical linear size of attack  $l_c(\alpha)$  for isotropic networks with linear sizes  $L = 50, 100, 150, 200$ , and characteristic link lengths  $\zeta = 3, 10$ . Figures (c) and (d) show  $l_c(\alpha)$  for anisotropic networks with  $\zeta = 3$  and  $\zeta = 10$ , respectively, and for  $\sigma = 0.25, 1$ . The existence of a preferred direction for the links ( $\theta_p = 0$ ), which causes the shortage of vertical connections, impairs the robustness of the system, since  $l_c$  decreases as  $\sigma$  decreases. The spatial embedding also debilitates the system and makes it easier to collapse when links are shorter. Note that the critical linear size  $l_c$  does not depend on the system length  $L$ , both for isotropic and anisotropic networks, with the exception of finite size effects for  $L = 50$ . These results were obtained by computing, by means of a binary search, the curve  $\alpha_c(l)$  from an average over  $N_{rea} = 20$  realizations, and then inverting this curve (see Fig. 11 in the SI section for the dispersion of these values).

an horizontal damage that disrupts the flow in the vertical direction of the network. That is, the GC does not extend between the top and bottom edges of the system. Regardless of the spatial embedding, we find that the critical attack size  $l_c$  decreases for networks with increasing anisotropy strength, i.e., for decreasing values of  $\sigma$ . In other words, the robustness of anisotropic systems gets reduced, compared to isotropic networks, as a result of the lack of connections in the vertical direction, which rapidly get lost, producing the fragmentation of the GC. This effect appears to be gradual when increasing the anisotropy levels (see Fig. 10 in the SI section). However, we expect that  $l_c \rightarrow 0$  as  $\sigma$  reaches a given minimum value, below which a GC that spans the whole system cannot be formed, prior to the localized attack, due to the insufficient amount of vertical links, i.e., being below the percolation threshold. In addition, and similar to isotropic networks, the critical linear size of attack does not depend on  $L$ , for large system sizes. We can associate the differences that the  $L = 50$  curve presents, in Fig. 3 (d), with respect to the results with larger  $L$ , to finite size effects, since networks have a large characteristic link length compared to  $L$  ( $\zeta = 10$ ) and the deviations appear more for large values of the attack size  $l$  too. Furthermore, it is plausible that the critical behavior of the system (isotropic or anisotropic) is governed only by the adimensional fraction between lengths  $l/\zeta$ . Indeed, our scaling results (see Fig. 9 in the SI section), suggest that such a scaling is a good approximation. However, more extensive computations and better statistics should be obtained in order to prove this assumption.

Lastly we analyze, at the end of the cascade process, all the connected clusters of nodes excluding the giant component, defined as the cluster touching all four edges of the system. First, in order to visualize the spatial distribution and orientation of these clusters, we plot them in Fig. 4. Figs. 4 (a) and (c), for  $\sigma = 0.25$  and  $\sigma = 1$ , respectively, show that the GC (in black) spans almost the entire network, *before* the localized attack (LA). On the other hand, at the *end* of the process triggered by the attack, the GC becomes fragmented and finite clusters appear, as seen in Figs. 4 (b) and (d). Note that in the latter figures we only considered clusters with sizes between 10 and 100 nodes, to clarify the image. We observe that the shape of the finite clusters change with the anisotropy of the system, and they can be located anywhere inside the network. For  $\sigma = 0.25$ , clusters are mostly horizontally stretched, while for more isotropic networks ( $\sigma = 1$ ), the clusters lose shape, as links can remain intact in many directions.

Next, in Figs. 5 (a) and (c) for  $\zeta = 3$  and  $\zeta = 10$ , respectively, we show the distribution

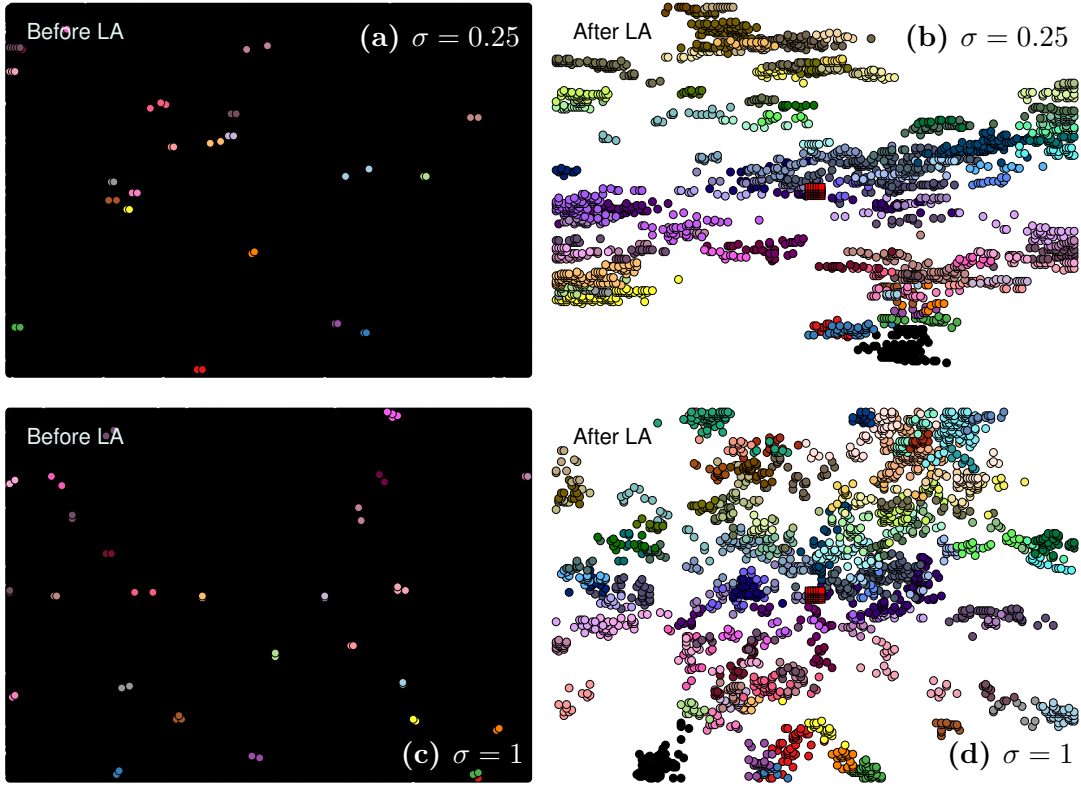


FIG. 4. Visualization of clusters before (left figures) and after (right figures) the localized attack (LA). In (a) and (b) we show an anisotropic network with  $\sigma = 0.25$ . From a GC that spans a huge part of the network (black region in (a)), we see that, after the LA, clusters retain some of the characteristic anisotropy, as they are rather stretched in the preferred horizontal direction. In (c) and (d) we present a more isotropic system, with  $\sigma = 1$ , in which the finite clusters, after the LA, do not have a defined shape. Note that red squares at the center of the networks in (b) and (d) represent the LA, of a square of linear size  $l = 6$ , while different clusters are depicted with circles of different colors. In order to simplify the display, in (b) and (d) we only show clusters with sizes between 10 and 100 nodes. The remaining parameters of the networks are  $L = 200$ ,  $\zeta = 3$ , and  $\alpha = 0.25$ . Clusters shown are the result of a single realization of networks and the corresponding attacks.

$n_s \equiv n_s(s)$  of cluster sizes, i.e., the probability of having a cluster of size  $s$ , prior to the localized attack. The attack of  $l = 6$ , which is above the critical size, triggers a cascade and affects the GC severely, changing the distribution  $n_s$ , as shown in Figs. 5 (b) and (d), for  $\alpha = 0.25$ . An interesting result that can be seen in Fig. 5 is that the final distribution of

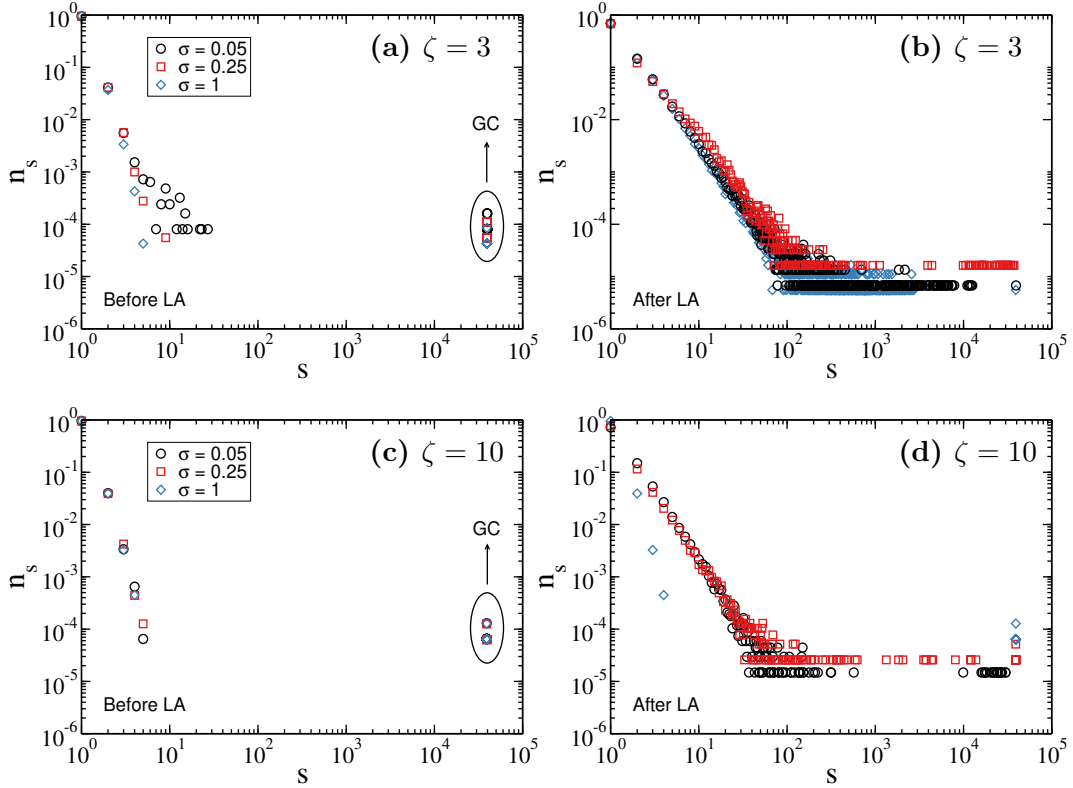


FIG. 5. Distribution of cluster sizes,  $n_s$ , before the localized attack (LA) of  $l = 6$  (left figures) and after the cascade triggered by it stops (right figures). In (a) and (b) we show  $n_s$  for  $\zeta = 3$ , while in (c) and (d) we show  $n_s$  for  $\zeta = 10$ . The localized attack triggers a CF process that changes the original distribution of cluster sizes. In (d), for  $\sigma = 1$ , the distributions before and after the LA are practically the same, which indicates that the tolerance  $\alpha = 0.25$  is large enough to avoid the disintegration of the GC due to cascading failures. This is consistent with the critical linear size of attack,  $l_c \approx 15$ , found in Fig. 3 (d). When the CF develops in the whole network, a power-law behavior is observed in the final distribution of cluster sizes, i.e.,  $n_s \sim s^{-\tau}$ , which suggests that the system is near the critical percolation state [17]. These results correspond to networks of linear size  $L = 200$ , averaged over  $N_{rea} = 70$  realizations.

cluster sizes,  $n_s$ , behaves like a power-law, i.e.,  $n_s \sim s^{-\tau}$ , with  $\tau > 0$ . Observation of the power-law in the cluster size distribution, at the end of the cascade, is expected because the cascading failures drive the system to the percolation critical point, at which the giant component disappears. Note that in the Motter and Lai model [1], the betweenness of nodes in a cluster is roughly proportional to the square of its size. As soon as the giant component

disappears, the cascading failures stop because the betweenness of each node drops below its maximal load.

Finally, we analyze the exponent  $\tau$  of the power-law. When fitting the initial trend of the data (up to  $s \sim 10^2$ ) using logarithmic binning we extract the exponents as shown in Fig. 6. For instance, in a network with strong spatial embedding ( $\zeta = 1$  in Fig. 6 (a)), the exponents

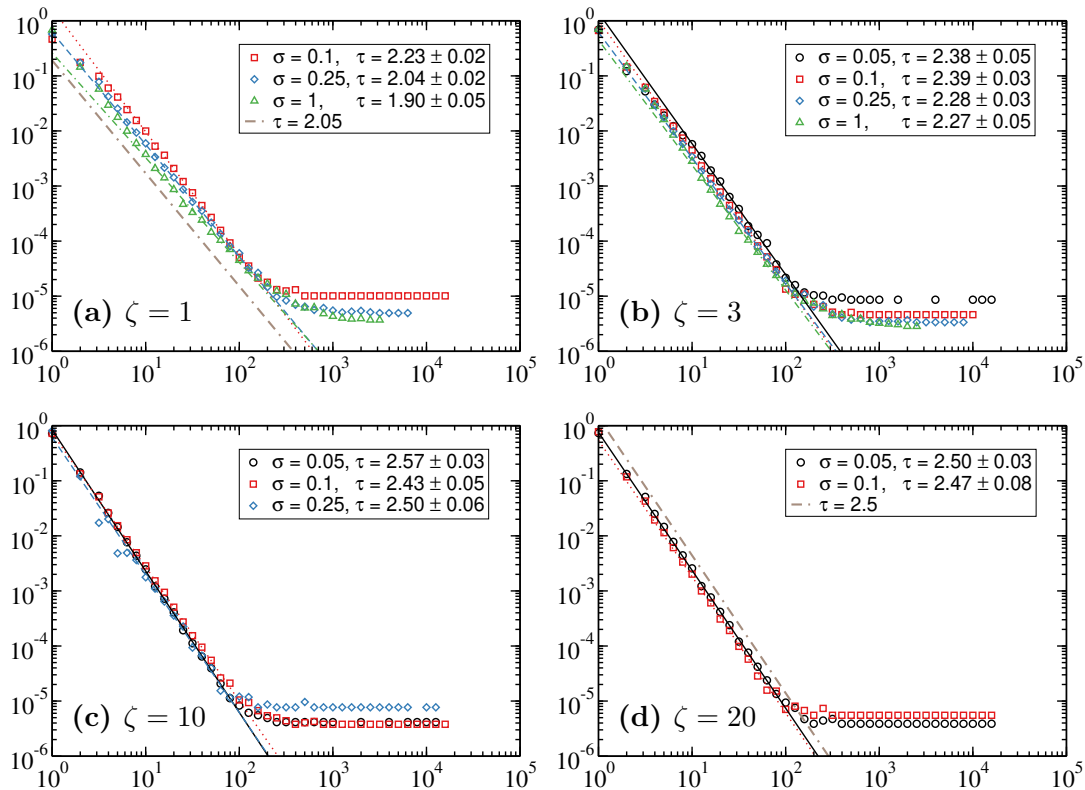


FIG. 6. Final distribution of cluster sizes  $n_s$ , corresponding to (a)  $\zeta = 1$ , (b)  $\zeta = 3$ , (c)  $\zeta = 10$ , and (d)  $\zeta = 20$ . The distribution behaves partly (due to finite systems) like a power-law  $n_s \sim s^{-\tau}$  (up to  $s \sim 10^2$ ). Note that, for a strong spatial embedding - (a)  $\zeta = 1$  -, the exponent  $\tau$  is similar to that of critical percolation in a 2D-lattice,  $\tau = 2.05$ , while for large  $\zeta$  of values 10 and 20, it approaches the value  $\tau = 2.5$ , corresponding to a random network with a Poisson degree distribution, i.e., mean field exponent. A logarithmic binning was applied to raw data, which allows a better perception of power-law behaviors. The remaining parameters of the networks are the same as in Fig. 5.

are close to the value  $\tau = 2.05$ , which corresponds to the known critical percolation exponent in two-dimensional lattices [4, 18]. Increasing the characteristic link length  $\zeta$ , the spatial effects decline, and the value of the power-law exponent tends to  $\tau = 2.5$  (Fig. 6 (d)), which

is characteristic of random networks with a Poisson degree distribution or high dimensional lattices [4, 18] (with dimension  $d \geq 6$ ). Note that for  $\zeta = 10$  and  $\sigma = 1$  there is no cascade in the network, due to its high tolerance levels. A similar situation occurs for  $\zeta = 20$  and  $\sigma = 0.25, 1$ , thus we did not include these cases in Fig. 6 (d).

#### IV. CONCLUSIONS

In this paper, we study the dynamic process of cascading failures induced by overloads in both isotropic and anisotropic spatial networks. We start the cascades from square shaped, localized attacks, removing  $l \times l$  nodes at the center of networks and analyze the effects of the characteristic length  $\zeta$  and the angular dispersion  $\sigma$  of links (which characterize the spatial embedding and the anisotropy of the system, respectively) on the process.

First, we study the evolution and spatial distribution of the failures, and find that anisotropy restricts the failures to spread mostly along the preferential direction. This is a result of the lack of connections in the orthogonal (vertical) direction, with respect to the preferred (horizontal) direction, so the former become easily overloaded.

Next, we find that there exists a critical damage linear size  $l_c$ , above which the giant component of functional nodes collapses. This critical size  $l_c$  increases with the tolerance  $\alpha$  and with the strength of the spatial embedding, i.e., for small values of  $\zeta$ . We find that anisotropy deteriorates the robustness of the system, as the shortage of vertical links produces a weak connection of the giant component along this direction, which become easily overloaded and fail. In addition, these results, both for isotropic and anisotropic networks, seem not to depend on the system size for large enough systems. Thus, in the thermodynamic limit, a *zero* fraction of localized failures yields a macroscopic transition. This is in marked contrast to random failures, where a fraction of the system size (infinite number of nodes in the thermodynamic limit) is needed to fail and cause a system collapse.

#### ACKNOWLEDGMENTS

IAP, CEL and LAB wish to thank to UNMdP (EXA 956/20), FONCyT (PICT 1422/2019) and CONICET, Argentina, for financial support. SH wishes to thank the Israel Science Foundation, the Binational Israel-China Science Foundation (Grant No. 3132/19), the BIU

Center for Research in Applied Cryptography and Cyber Security, NSF-BSF (Grant No. 2019740), the EU H2020 project RISE (Project No. 821115), the EU H2020 DIT4TRAM, and DTRA (Grant No. HDTRA-1-19-1-0016) for financial support. D.V. thanks the PBC of the Council for Higher Education of Israel for the Fellowship Grant. S.V.B acknowledges the partial support of this research through the Dr. Bernard W. Gamson Computational Science Center at Yeshiva College. This research was supported by a grant from the United States-Israel Binational Science Foundation (BSF), Jerusalem, Israel (Grant No. 2020255).”

---

- [1] A. E. Motter and Y.-C. Lai, *Phys. Rev. E* **66**, 065102 (2002).
- [2] Y. Berezin, A. Bashan, M. Danziger, L. Daqing, and S. Havlin, *Scientific reports* **5**, 8934 (2015).
- [3] M. E. J. Newman, *Networks: An Introduction* (Oxford University Press, 2010).
- [4] A. Bunde and S. Havlin, *Fractals and disordered systems* (Springer-Verlag New York, Inc., 1991).
- [5] Y. Kornbluth, G. Barach, Y. Tuchman, B. Kadish, G. Cwilich, and S. V. Buldyrev, *Phys. Rev. E* **97**, 052309 (2018).
- [6] I. Dobson and L. Lu, *IEEE Transactions on Circuits and Systems I: Fundamental Theory and Applications* **39**, 762 (1992).
- [7] I. Dobson, B. A. Carreras, V. E. Lynch, and D. E. Newman, *Chaos: An Interdisciplinary Journal of Nonlinear Science* **17**, 026103 (2007).
- [8] B. A. Carreras, D. E. Newman, and I. Dobson, *IEEE Transactions on Power Systems* **31**, 4406 (2016).
- [9] J. Zhao, D. Li, H. Sanhedrai, R. Cohen, and S. Havlin, *Nature communications* **7**, 1 (2016).
- [10] D. Vaknin, M. M. Danziger, and S. Havlin, *New Journal of Physics* **19**, 073037 (2017).
- [11] B. M. Waxman, *IEEE J. Sel. Areas Commun.* **6**, 1617 (1988).
- [12] L. Daqing, K. Kosmidis, A. Bunde, and S. Havlin, *Nature Physics* **7**, 481 (2011).
- [13] National Land Information Division, National Spatial Planning and Regional Policy Bureau, MILT of Japan, National railway data (2012).
- [14] M. M. Danziger, L. M. Shekhtman, Y. Berezin, and S. Havlin, *EPL (Europhysics Letters)* **115**, 36002 (2016).



- [15] S. Havlin, L. A. Braunstein, S. V. Buldyrev, R. Cohen, T. Kalisky, S. Sreenivasan, and H. Eugene Stanley, *Physica A* **346**, 82 (2005).
- [16] D. Vaknin, B. Gross, S. V. Buldyrev, and S. Havlin, *Phys. Rev. Research* **2**, 043005 (2020).
- [17] A. Coniglio, *Journal of Physics A: Mathematical and General* **15**, 3829 (1982).
- [18] D. Stauffer and A. Aharony, *Introduction to Percolation Theory* (Taylor & Francis, 1994).

## V. SUPPLEMENTARY INFORMATION

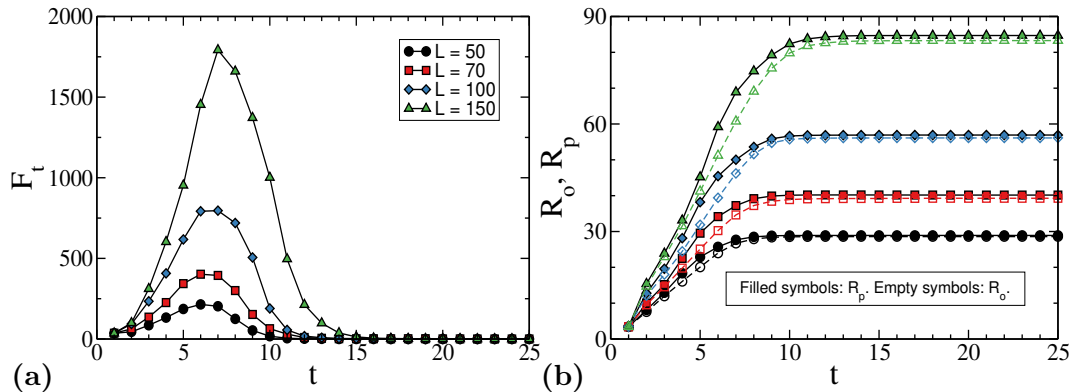


FIG. 7. **Consistency with isotropic model.** (a) Amount of failures  $F_t$  at time  $t$ , for different values of the lattice-length  $L$ . (b) Estimation of the extent of the failures in the preferential ( $\theta_p = 0$ ) and orthogonal ( $\theta = \pi/2$ ) directions,  $R_p$  and  $R_o$ , respectively, for the same values of  $L$  than in (a). These results correspond to networks with strong spatial embedding ( $\zeta = 1$ ) and low anisotropy ( $\sigma = 1$ ), in which periodic boundary conditions were introduced, and which resemble the isotropic lattices used in Ref. [9]. To be consistent with the measure of the magnitude  $r_c(t)$  in [9], the radius  $R_p$  and  $R_o$  are multiplied by 2, to comprise approximately 95% of all failures and, thus, represent the extent of the failures at time  $t$ . Our results are in well agreement with those obtained in the cited work. However, small differences appear due to the fact that our network is not a perfect lattice, and because of the different methodology for measuring the spatial distribution of the failures. Notice that the velocity of failure spreading (i.e., the slope of the radius), besides being approximately constant, is virtually the same both in the preferential and the orthogonal direction, given the low anisotropy of the network. The remaining parameters of the simulation are  $\alpha = 0.25$ , and  $l = 6$ . Results were averaged over  $N_{rea} = 50$  realizations.

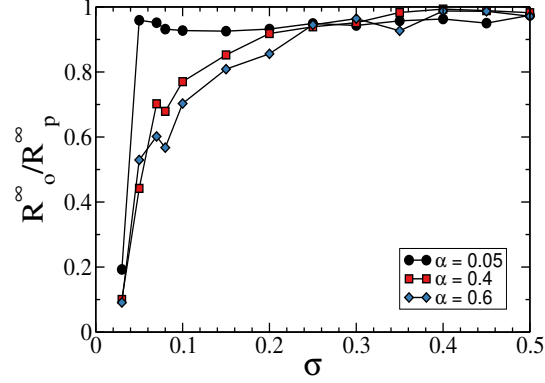


FIG. 8. **Ratio**  $R_o^\infty/R_p^\infty$ . We show the ratio between the extents of the failures in the orthogonal ( $\theta = \pi/2$ ) and preferential ( $\theta_p = 0$ ) directions, at the end of the cascade, for the same networks as in Fig. 2 (c), but for different values of the tolerance  $\alpha$ . We observe that the decay of  $R_o^\infty/R_p^\infty$ , in the limit of completely anisotropic networks ( $\sigma \rightarrow 0$ ), is more abrupt as  $\alpha$  decreases since all nodes are more susceptible to fail.

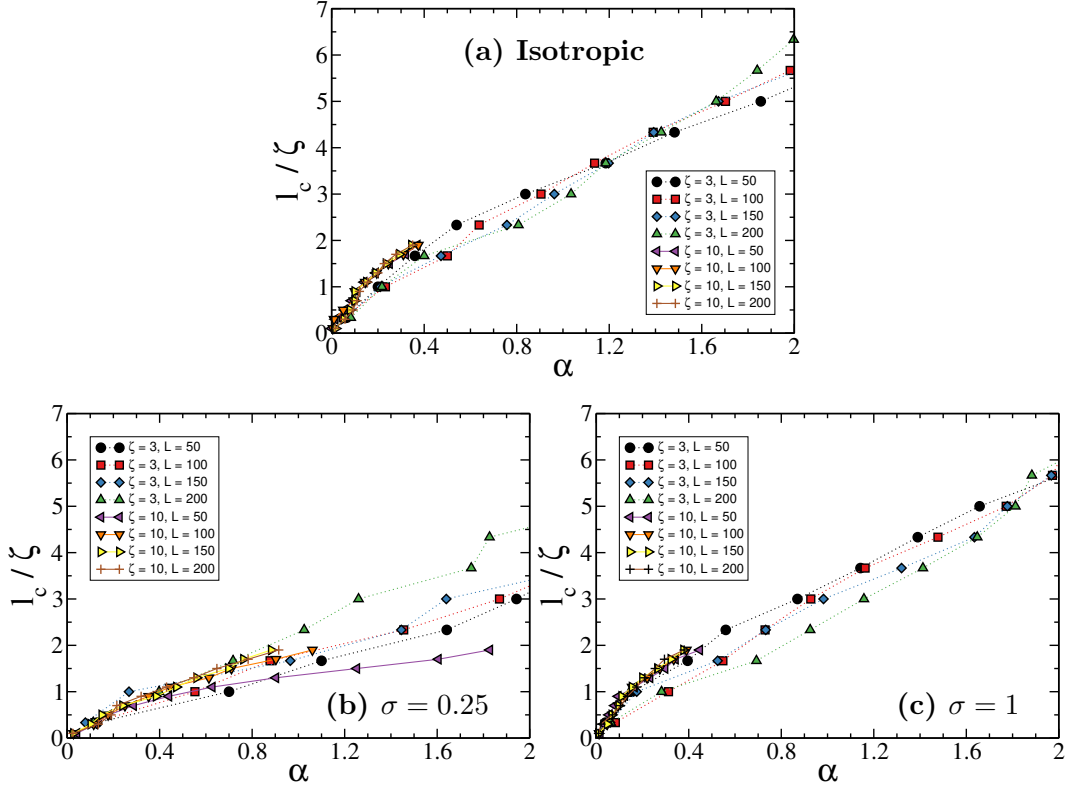


FIG. 9. **The critical behavior for the scaled  $l_c$ .** Here we take results presented in Fig. 3 and divide the critical attack length  $l_c$  by the characteristic link-length  $\zeta$ . The curves for the different values of  $\zeta$  appear to approximately collapse, which suggests that the adimensional quotient  $l_c/\zeta$  rules the behavior of the system at the criticality. The deviation from a single curve might be due to not enough statistics and due to small systems like  $L = 50$ . Therefore, more extensive computations should be carried away to assess this properly, e.g., attacks with  $l > 20$  should be explored in networks with  $\zeta = 10$  in order to get results for bigger  $\alpha$  values, as well as increase the amount of realizations and the system size  $L$ .

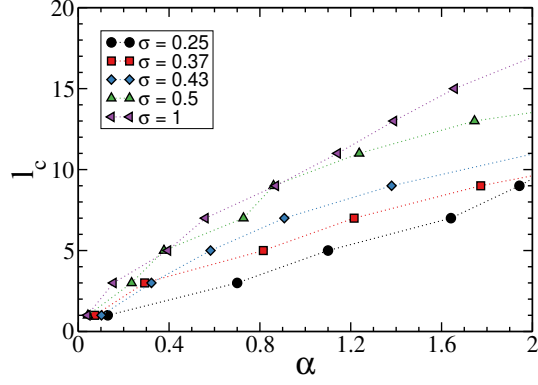


FIG. 10. **Variation of  $l_c(\alpha)$  with  $\sigma$ .** We present here the critical attack length  $l_c(\alpha)$  for different values of the anisotropy parameter  $\sigma$ , in networks with  $L = 50$  and  $\zeta = 3$  (see Fig. 3 (c)). These curves suggest that the changes introduced by the anisotropy are gradual, taking the critical values to zero as  $\sigma$  decreases and reaches a minimum value, for which there is no GC in the system due to the lack of vertical connections.

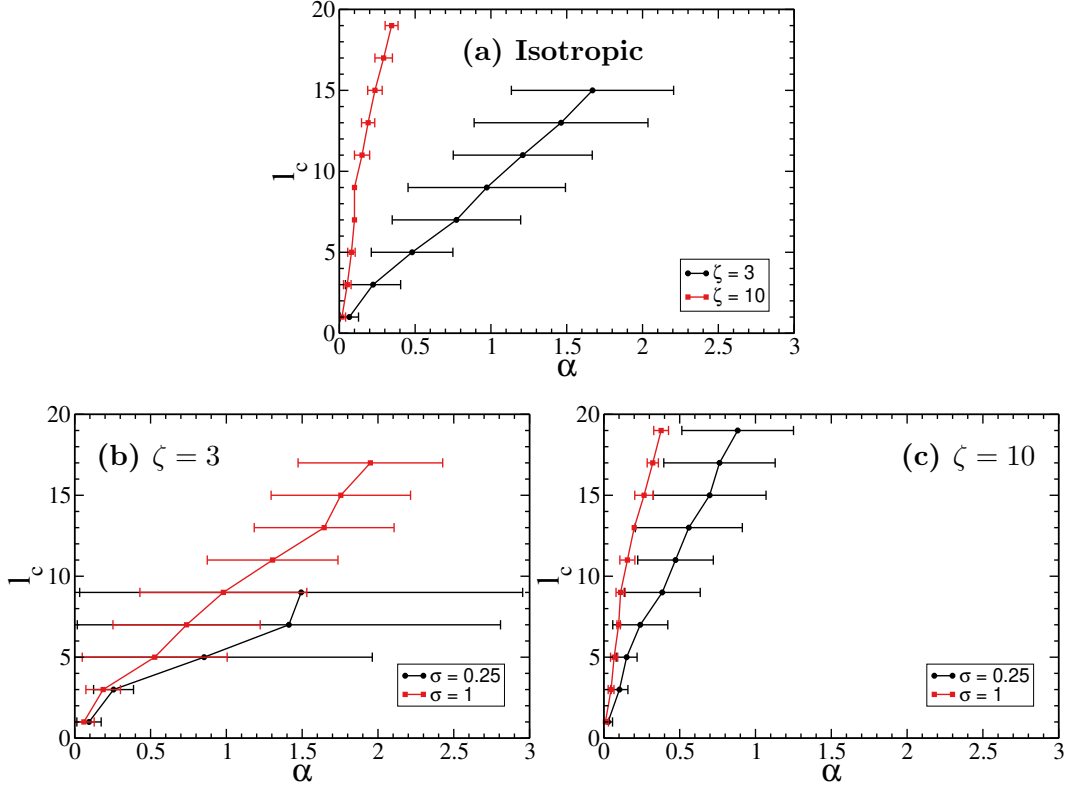


FIG. 11. **Standard deviation for  $l_c(\alpha)$ .** We show the dispersion along the horizontal axis since we computed, first,  $\alpha_c(l)$  and then inverted the curve. (a) Isotropic networks with  $\zeta = 3, 10$ . (b)-(c) Anisotropic networks with  $\zeta = 3$  (left) and  $\zeta = 10$  (right), for  $\sigma = 0.25, 1$ . All the results correspond to different realizations of networks with linear size  $L = 150$ .